Nonuniform Dust Outflow Observed around Infrared Object NML Cygni

J. D. Monnier, M. Bester, W. C. Danchi, M. A. Johnson[1], E. A. Lipman, C. H. Townes, and P. G. Tuthill

Space Sciences Laboratory, University of California, Berkeley, Berkeley, CA 94720-7450, USA

T. R. Geballe

Joint Astronomy Centre, 600 North A'ohoku Place, University Park, Hilo, HI 96720, USA

D. Nishimoto

Rockwell Power Systems, 535 Lipoa Parkway, Suite 200, Kihei, HI 96753, USA

P. W. Kervin

USAF Phillips Laboratory, 535 Lipoa Parkway, Kihei, HI 96753, USA

ABSTRACT

Measurements by the University of California Berkeley Infrared Spatial Interferometer at 11.15 μm have yielded strong evidence for multiple dust shells and/or significant asymmetric dust emission around NML Cyg. New observations reported also include multiple 8-13 μm spectra taken from 1994-1995 and N band (10.2 μm) photometry from 1980-1992. These and past measurements are analyzed and fitted to a model of the dust distribution around NML Cyg. No spherically symmetric single dust shell model is found consistent with both near- and mid-infrared observations. However, a circularly symmetric maximum entropy reconstruction of the 11 μm brightness distribution suggests a double shell model for the dust distribution. Such a model, consisting of a geometrically thin shell of intermediate optical depth ($\tau_{11\mu\mathrm{m}} \sim 1.9$) plus an outer shell ($\tau_{11\mu\mathrm{m}} \sim 0.33$), is consistent not only with the 11 μm visibility data, but also with near-infrared speckle measurements, the broadband spectrum, and the 9.7 μm silicate feature. The outer shell, or large scale structure, is revealed only by long-baseline interferometry at 11 μm, being too cold ($\sim$400 K) to contribute in the near-infrared and having no unambiguous spectral signature in the mid-infrared. The optical constants of Ossenkopf, Henning, & Mathis (1992) proved superior to the Draine & Lee (1984) constants in fitting the detailed shape of the silicate feature and broadband spectrum for this object. Recent observations of H_2O maser emission around NML Cyg by Richards, Yates, & Cohen (1996) are consistent with the location of the two dust shells and provide further evidence for the two-shell model.

[1]on leave from Lawrence Livermore National Laboratory, 7000 East Avenue, P.O. Box 808, L-463, Livermore, CA, 94550, USA

1. Introduction

NML Cyg is believed to be a supergiant surrounded by an optically thick, dusty envelope. An oxygen-rich atmosphere is evidenced in the mid-infrared spectrum by the presence of a silicate feature in partial absorption. The high optical depth of the enshrouding material is clearly shown by the extreme redness of the broadband spectrum. This spectrum has been fitted by Rowan-Robinson & Harris (1983) by modeling the circumstellar environment as a single shell of dirty silicate dust, assuming a spherically symmetric, uniform outflow. A uniform outflow would produce a $\rho_{\rm dust} \propto r^{-2}$ dust density distribution, assuming the dust is accelerated to its terminal velocity near the star. Observations of a dust distribution not consistent with $\rho_{\rm dust} \propto r^{-2}$ would imply the mass loss varies with time and may reveal new information about the physical processes involved, such as the relevant time and length scales.

A target of early workers in speckle interferometry, NML Cyg has had its angular size measured at various infrared wavelengths (Sibille, Chelli, & Lena 1979; Dyck et al. 1984; Ridgway et al. 1986; Fix & Cobb 1988; Dyck & Benson 1992). Ridgway et al. (1986) demonstrated that the near-infrared visibility measurements can be explained by a dust shell geometry similar to that in the uniform outflow model of Rowan-Robinson & Harris (1983), however this new model did require the introduction of excess stellar flux, presumably escaping through less dense regions in the dust envelope or by excess forward-scattering off of grains.

Other workers (Rowan-Robinson 1982; Rowan-Robinson & Harris 1983; David & Papoular 1990, 1992), while finding uniform outflow models to be consistent with giants whose silicate feature is in emission where the dust is optically thin, have found indications of other dust shell geometries for optically thick envelopes. NML Cyg belongs to neither group, its silicate feature not evincing strong emission nor deep absorption. Dynamical simulations of the extended envelopes of carbon stars by Winters et al. (1994, 1995) and Fleischer, Gauger, & Sedlmayr (1995) show multiple shell structures caused by an interplay of the dust formation process and the underlying stellar pulsation. Such structures are also expected to arise in the atmospheres of oxygen-rich stars.

This paper introduces new 11.15 μm observations of the dust shell around NML Cyg with the U.C. Berkeley Infrared Spatial Interferometer (ISI), recent measurements of the mid-infrared spectrum using the United Kingdom Infrared Telescope (UKIRT), and systematic long-term N Band (10.2 μm) photometry at the Maui Space Surveillance Site. Radiative transfer calculations were performed to determine whether previously published models of the circumstellar dust shell were consistent with these new data. We were unable to produce a uniform outflow model which could fit both the new and previously published observations; however, a double shell model satisfactorily does so.

Uniform outflow and spherical symmetry are usually assumed in the modeling of evolved stars since the lack of high resolution imaging data does not require a more detailed model (see Lopez et al. 1997 for recent modeling efforts not assuming spherical symmetry). These simplifications will come under greater scrutiny as the dust envelopes are imaged at successively higher resolution. Given the known gas velocities ($\sim$5-30 km/s) and estimated distances of close red giants ($\sim$100-200 pc), dust will move across one ISI "resolution element" of 30 mas in a time scale of order the star's pulsational period ($\sim$400 days). This suggests that any pulsation-related inhomogeneities associated with the mass loss mechanisms can be observed by the ISI, assuming velocity gradients are not large enough to disperse the dust into an an average r^{-2} density distribution. With a CO outflow velocity measured to be $\sim$25 km/s (Knapp et al. 1982; Bowers, Johnston, & Spencer 1983; Morris & Jura 1983), NML Cyg's greater distance of approximately 1800 pc (Bowers et al. 1983; Morris & Jura 1983; Richards et al. 1996) and longer pulsational period of $\sim$940 days as determined from N band photometry (Figure 1) imply that the highest resolution spatial structure observed by the ISI corresponds to a temporal scale of $\sim$10 yrs ($\sim$3 cycles), making observations of pulsation-related dust inhomogeneities possible.

2. Observations

2.1. Mid-Infrared Visibility Measurements

NML Cyg was observed in July and September of both 1993 and 1994 and in September and October of 1996 by the U.C. Berkeley Infrared Spatial Interferometer (ISI). The ISI is a two-element, heterodyne stellar interferometer operating at discrete wavelengths in the 9-12 μm range and is located on Mt. Wilson, CA. The telescopes are each mounted within a movable semi-trailer and together can currently operate at baselines ranging from 4 to 35 m. Detailed descriptions of the apparatus and recent upgrades can be found in Bester et al. (1990, 1994). System calibration was maintained with the observations of partially resolved K giant stars α Tau and α Boo which have no dust known to be surrounding them. Uncalibrated visibilities were found to drift approximately 15% from year to year, thus larger systematic uncertainties may be present when comparing data from different years. Extended discussions of calibration issues and uncertainties are found in Danchi et al. (1990, 1994a). A journal of NML Cyg observations is provided in Table 1 and contains the final calibrated visibilities along with error bounds representing the statistical uncertainty of each visibility measurement (corresponding to $\sim$15 minutes of on-source integration in most cases). Note that the measurement at the longest baseline yielded only an upper bound to the visibility. The diffraction-limited beam size is $\sim 1\farcs5$, which does not affect the interpretation of the visibility curves since previous 10 μm speckle measurements (Fix & Cobb 1988; Dyck & Benson 1992) have indicated that essentially all the mid-infrared emission arises from a region 5 times smaller than this ($\Theta_{\rm FWHM} \sim 0\farcs3$).

2.2. Long-term N Band Photometry

N band (10.2 μm) photometry of NML Cyg from the Maui Space Surveillance Site (MSSS) (Nishimoto et al. 1995) is presented in Figure 1. These data were secured as part of a program monitoring a number of late-type stars from 1980 to 1992 for the purpose of calibrating an infrared radiometer system, typically using an N Band equivalent filter. The MSSS radiometer, installed on a 1.2 m telescope, consisted of a square array of 25 cadmium-doped germanium (Ge:Cd) photoconductive detectors cooled to 12 K. All reported measurements are included in Figure 1 and show large fluctuations ($\sim$0.3 mag) from day to day. Two effects contributed to this large uncertainty. Firstly, the MSSS often operated under atmospheric conditions considered non-photometric by astronomical observatories. Secondly, the integration time for each measurement was limited due to the large number of objects being surveyed each night. However, the large data volume available ($\sim$1000 independent measurements over 12 years) allowed these problems to be mitigated by binning the data into 30 day windows, with the median of each bin yielding a magnitude estimate insensitive to the effects of outlying points caused by non-photometric conditions. These median data points depicted on Figure 1 confirm Strecker's (1975) report of a long-term periodicity of $\sim$1000 days. The peak-to-trough N band amplitude is $\sim$0.5 mag, slightly smaller than the $\sim$0.6 mag variation reported by Strecker at 3.5 μm in the early 1970s. The average period, as measured from the MSSS photometry, is $\sim$940 days, although inspection of the light curve reveals that NML Cyg is not a regular pulsator.

2.3. Mid-infrared Spectrophotometry

More recent mid-infrared photometry was carried out with the United Kingdom Infrared Telescope (UKIRT) from 1991 to 1995. Both narrowband photometry (using the single-channel bolometer in UKT8) and 8-13 μm spectrophotometry (using the linear array spectrometer CGS3) have been obtained with $5''$ diameter apertures and standard chopping and nodding techniques. Flux calibrations were derived from observations of α Lyr, α Aur, α CMa, and other bright standard stars. In all but one case the intercomparison of standards on a given night were internally consistent to within several percent, and hence it is believed that on those nights the flux level determined for NML Cyg is accurate to $\pm$10% or better. On 1994 November 20, which was not photometric, the uncertainty is probably $\pm$20%. Details of the spectral shape of NML Cyg are least reliable near 9.7 μm, due to strong telluric absorption by ozone. Wavelength calibrations were derived from observations of a krypton arc lamp in 4th, 5th, and 6th order, and are accurate to $\pm$0.02 μm.

The flux densities at 11.15 μm, the wavelength at which the ISI observations were obtained, are listed in Table 2, while plots of all spectra can be found in Figure 2. The shape of the silicate feature was nearly constant in all observations despite variations in the total stellar flux, with the possible exception of the spectra taken near minimum luminosity. Based on the MSSS N band photometry, the 1995 August 20 UKIRT data were chosen to represent the "mean" mid-infrared spectrum of NML Cyg and appear in Figures 3b and 5b. All the UKIRT mid-infrared photometry were converted to equivalent N band magnitudes and are plotted on Figure 1 for comparison with the MSSS photometry. The two data sets from UKIRT and MSSS overlap in time during Fall 1991, and yield internally consistent flux measurements to within known uncertainties.

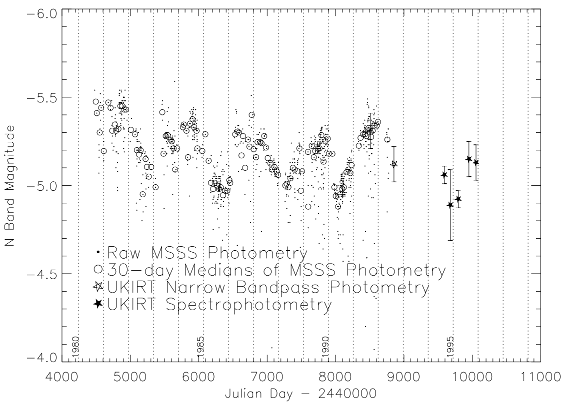

Fig. 1.— The N band (10.2 μm) magnitude of NML Cyg from 1980 to 1996. The raw data from the Maui Space Surveillance Site (MSSS) are presented as dots, while the circles are the medians of the raw data binned into 30 day windows. The open stars are N band equivalent flux determinations derived from narrow band UKIRT observations at 10.5 μm and 11.5 μm. The filled stars were derived from 8-13 μm UKIRT spectrophotomery. The flux varies ±0.25 magnitudes with an irregular period of $\sim$940 days.

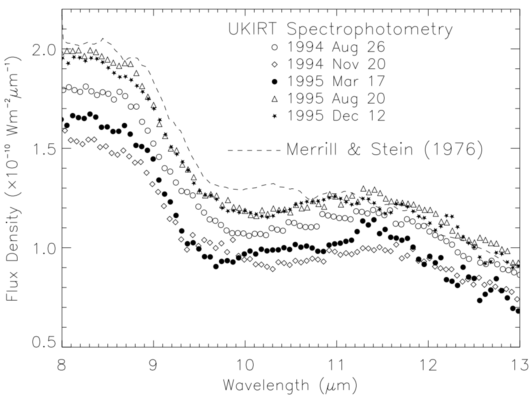

Fig. 2.— The 8-13 μm spectrum of NML Cyg at 5 recent epochs (plot symbols) along with a previously published spectrum from 1976 scaled to the present mean flux level (dashed line). The UKIRT spectrophotometric data were collected on 1994 Aug 26 (open circles), 1994 Nov 20 (diamonds), 1995 Mar 17 (filled circles), 1995 Aug 20 (triangles), and 1995 Dec 12 (filled stars). The shape of the silicate feature changed little during the last pulsational cycle and appears very similar to a previous measurement taken over 20 years ago.

3. Modeling Procedure

3.1. Modeling Code

One goal of this work is to develop a model of the circumstellar environment of NML Cyg which can explain both new and previously published observations. This requires a method for calculating the visibility curves and spectra from a given a set of model parameters. The radiative transfer modeling code used for this purpose was based on the work of Wolfire & Cassinelli (1986) and assumes the dust distribution to be spherically symmetric (see Danchi et al. [1994a] for a detailed description). Starting with the optical properties and density distribution of the dust shell, this code calculates the equilibrium temperature of the dust shell as a function of the distance from the star, whose spectrum is assumed to be a blackbody. Subsequent radiative transfer calculations at 67 separate wavelengths allow the wavelength-dependent visibility curves, the broadband spectral energy distribution, and the mid-infrared spectrum all to be computed for comparison with observations. The dense sampling of the silicate band is particularly useful for comparison with UKIRT spectrophotometry. For a uniform outflow model of the dust shell, a Sun Sparcstation 10 could perform this calculation within 2 minutes, while more complex geometries, such as those including multiple dust shells, generally took $\sim$5 minutes.

The code treats a distribution of dust sizes by calculating the dust temperature as a function of grain size and dust type (e.g. dirty silicates, amorphous carbon, graphite), using the Mathis, Rumpl, & Nordsieck (1977) grain size distribution, where the number density $n \propto a^{-3.5}$, and grain size spanned $0.01\,\mu\text{m} < a < 0.25\,\mu\text{m}$. The wavelength-dependent grain opacity, when averaged over the grain size distribution, was found to be insensitive to the exact choice of the grain size cutoffs for wavelengths above 1 μm. Dust opacities were calculated from the optical constants assuming spheroidal Mie scattering using a method developed by Toon & Ackerman (1981).

For stars having oxygen-rich atmospheres, it is appropriate to use optical constants for astronomical silicates. Previous analyses of oxygen-rich envelopes using the ISI visibility data (e.g. Danchi et al. 1994a,b) have utilized the Draine & Lee (1984) optical constants for astronomical silicates when computing the spectrum. Recent mid-infrared spectra from UKIRT of late-type stars present the opportunity to test these constants more rigorously.

The optical constants of Draine & Lee (DL 1984), Ossenkopf, Henning, & Mathis (OHM 1992), and David & Papoular (DP 1990), were all used in modeling the dust shell of NML Cyg. Calculations of the silicate feature using DL constants could not reproduce the observed spectral shape, while the more recently determined optical constants of DP and OHM were successful at matching observations. Although OHM and DP constants both provided similar high-quality fits to the shape of the silicate feature, OHM dust proved superior in reproducing the shape of the observed near-infrared spectrum. The OHM constants in the near-infrared were determined for laboratory silicates with metallic inclusions (iron and iron-oxide), leading to a higher opacity (relative to the silicate feature) than both the DL and DP constants. We were unable to produce models using the DL or DP optical constants which matched the excellent fits resulting from the OHM constants, and hereafter all results presented are those obtained using the OHM optical constants.

Radio observations suggest that NML Cyg is at a distance of approximately 1800 pc (Bowers et al. 1983; Morris & Jura 1983; Richards et al. 1996) in an OB association (Cyg OB2). At this distance, attenuation in the visible and near-infrared due to intervening interstellar material is significant, and has been measured by Lee (1970) who found $E_{\mathrm{B-V}}$ to be $\sim$1.2 in the direction of Cygnus. Thus before comparison with observations, simulated spectra were reddened following Mathis (1990) with $R_{\mathrm{V}} = 3.1$, yielding a transmission of 25% at 1 μm, 64% at 2 μm, and 92% at 5 μm.

3.2. Published Observations

The new observations of NML Cyg are important in defining models, but are unable, by themselves, to adequately constrain the range of acceptable dust envelope geometries. To this end, a literature search was conducted in an effort to compile a more comprehensive data set for comparison with the simulated visibility curves and spectra. In fitting all of the compiled data, new observations were given priority over previously published measurements because secular changes in NML Cyg's observables may have occurred, rendering older data less representative of current conditions.

This section briefly discusses three sets of published data which were used to guide the modeling process and which appear in our figures: mid-infrared speckle data, near-infrared speckle data, and wide-bandpass spectral measurements of NML Cyg.

The high-resolution 11.15 μm visibility data were complemented at low spatial resolution by observations employing mid-infrared speckle interferometry. Fix & Cobb (1988) first performed this type of measurement in 1985 at the 3 m NASA Infrared Telescope Facility (IRTF) and Dyck & Benson (1992) repeated it using narrowband filters in 1988 and 1989 at the 2.4 m Wyoming Infrared Observatory. These results all agree to within uncertainties, and have been plotted in Figures 3a and 5a, while observational details are summarized in Table 3.

Sibille et al. (1979), Dyck et al. (1984), and Ridgway et al. (1986) have all obtained near-infrared speckle interferometric measurements. The wavelengths, passbands, and dates of all three observations can be found in Table 3, while the results are plotted in Figures 3c and 5c. The formal error bars are approximately the same size as the plot symbols or smaller, although the results from the three papers usually do not agree with each other to within the quoted uncertainties. This disagreement may reflect real changes in the size of NML Cyg between the different measurements, or represent inadequate calibration for the atmospheric seeing. Ridgway et al. (1986) presented the most recent and highest resolution set of observations, and these are given greater weight in the model fitting. However, the highest resolution points of this data generally show a trend towards higher visibility. According to the authors, the presence of broadband noise proportional to stellar flux can cause this effect, so following their example, we did not attempt to fit data beyond approximately 0.75 of the telescope cutoff (see Figures 1 and 2 of Ridgway et al. [1986]). However, the entire data sets are presented in Figures 3c and 5c with a dotted, vertical line showing the position of the spatial frequency cutoff.

The last data set used in the modeling procedure was comprised of broadband spectra of NML Cyg. Since NML Cyg has demonstrated variability in the mid-infrared, it was desirable to find data containing a broad range of frequency measurements all taken at the same, recent epoch. Unfortunately, the most recent spectrum located in the literature was from Dyck, Lockwood, & Capps (1974), and the fluxes taken from this paper, along with fluxes from Johnson, Low, & Steinmentz (1965), are given in Figures 3b and 5b. These groups collected their measurements over a period of 10 and 20 days respectively, thus allowing for direct intra-comparison. The Dyck et al. flux measurements were taken near 1971 September 20, while Johnson et al. observations were tekn around 1965 May 7. The error bars represent statistical measurement uncertainties, but an additional 10% uncertainty associated with the absolute calibration has not been plotted. Strecker's (1975) light curve clearly shows NML Cyg to be near its 3.5 μm minimum at the time of the Dyck et al. measurement, and the absolute flux reported by the two groups agree to within uncertainties. The phase of NML Cyg during the Johnson et al. measurement can not be extrapolated since NML Cyg has an irregular period; however, the 1971 data is systematically lower than the 1965 data, consistent with September 1971 marking a minimum in stellar luminosity. The $\lambda = 10.2\,\mu$m data points provide an unexplained exception to this trend, indicating perhaps a larger uncertainty in the Johnson et al. measurement than claimed by the authors.

4. Single Shell Models

Both Rowan-Robinson & Harris (1983) and Ridgway et al. (1986) have modeled the circumstellar environment of NML Cyg as a single dust shell undergoing uniform outflow. By also assuming that the dust is accelerated to a terminal velocity through a distance which is small compared to the dust shell's full extent, one can approximate the density distribution as $\rho \propto r^{-2}$. In this model, no dust is presumed to exist between the stellar surface and the dust shell's inner radius, the location at which dust condenses out of the gas phase. Both groups concluded that the available data could be accurately reproduced by such a model if the inner radius is chosen to be $\sim$ 40 mas from the star. To test this scenario, a series of models was constructed in which the inner radius of the dust shell was fixed at 40 mas, while the total optical depth was varied.

The solid line in Figure 3, corresponding to an 11.15 μm optical depth of 2.4, was the result of fitting only to the broadband spectrum. Note the reasonable agreement with the 11.15 μm high resolution visibility data, although the observed mid-infrared size, as measured by the low resolution speckle observations, is smaller than the model predicts. Interestingly, the observed angular diameters at 3.6 μm and 4.8 μm show the opposite trend, being larger than the model simulations. Table 4 contains a summary of the model parameters. The dust temperature at the inner radius for this model was $\sim$ 1200K, consistent with the expected condensation temperature for astronomical silicates.

Further note from Figure 3b that the observed silicate feature is only partly reproduced by this uniform outflow model. Although the results were not plotted, further calculations revealed that a nearly perfect fit to the silicate feature could be achieved by increasing the optical depth from 2.4 to 3.9. However, this increase in optical depth severely cut off the broadband spectrum below 2 μm and also enhanced the 10 μm emission region, worsening the fit to the mid-infrared speckle interferometric measurements.

One plausible scenario which accounts for the high optical depth, while simultaneously avoiding problems with the visible and near-infrared spectrum, is that there exist holes, or weak spots, in the dust shell allowing more stellar flux to escape than expected from the "mean" optical depth. A similar effect would be caused by enhanced forward scattering by the grains. These possibilities alleviate the problems of fitting the broadband and near-infrared visibility curves, and Ridgway et al. (1986) were able to fit their near-infrared visibility curves by treating the fractional stellar flux as a free parameter. However, these scenarios are not consistent with the recent mid-infrared observations. The 4.8 μm optical depth assumed in the Ridgway et al. (1986) paper is $\sim$ 4 times larger than in our best fitted uniform outflow model (solid line, Figure 3). Uniform outflow models with optical depths roughly matching those of Ridgway were produced for comparison with mid-infrared observations. Significantly, no such model was found which could reconcile the relatively small overall size of the mid-infrared emission region of NML Cyg, as indicated by the low resolution speckle measurements, with the large size implied by the high optical depth of the Ridgway et al. (1986) model. Another observation which is difficult to explain with a model characterized by high optical depth and a large unresolved flux component is the shape of the silicate feature. Using OHM optical constants, a simulation of such an optically thick dust shell ($\rho_{\rm dust} \propto r^{-2}$) predicted a significantly deeper absorption feature centered around 9.7 μm than was actually observed.

The major conclusions drawn by comparing these

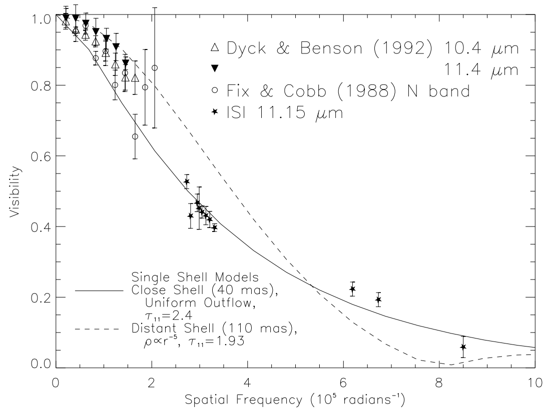

Fig. 3a.— The predictions of single shell models are compared to a set of new and previously published observations. The solid line represents results from a single shell, uniform outflow model of the dust distribution around NML Cyg, while the dashed line arises from a model of a single, geometrically thin shell (see Table 4). (a) Numerical models are compared with 11 μm visibility data. Neither model can fit the short- and long-baseline data simultaneously.

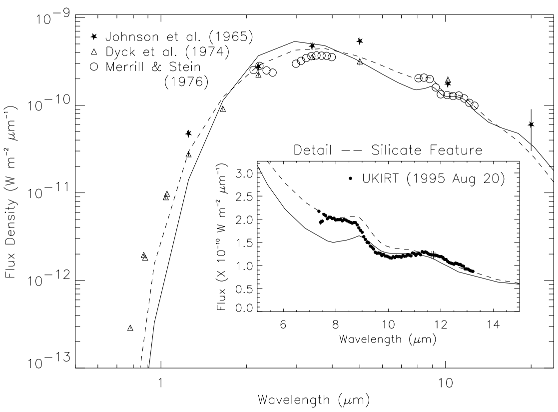

Fig. 3b.— The predictions of single shell models are compared to a set of new and previously published observations. The solid line represents results from a single shell, uniform outflow model of the dust distribution around NML Cyg, while the dashed line arises from a model of a single, geometrically thin shell (see Table 4). (b) The model spectra are compared to broadband and mid-infrared spectral measurements. The geometrically thin shell model (dashed line) fits these observations much better than the uniform outflow model (solid line).

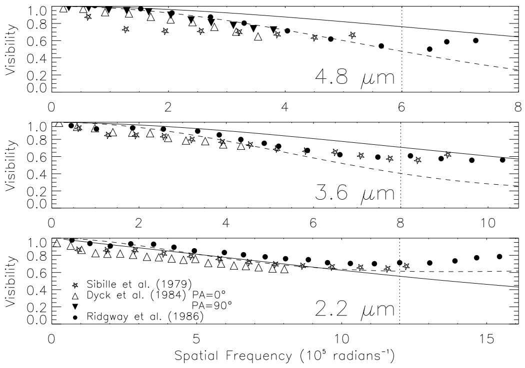

Fig. 3c.— The predictions of single shell models are compared to a set of new and previously published observations. The solid line represents results from a single shell, uniform outflow model of the dust distribution around NML Cyg, while the dashed line arises from a model of a single, geometrically thin shell (see Table 4). (c) Previously published near-infrared visibility measurements near 4.8 μm, 3.6 μm, and 2.2 μm are compared to model calculations. Error bars are not plotted but are comparable to the size of each data point or smaller. Again, the geometrically thin shell model (dashed line) proves superior in reproducing observations. The vertical dotted line represents the spatial frequency cutoff discussed in §3.2.

previous models with the current data set are:

1. Uniform outflow models with dust shell inner radii of 40 mas are not consistent with 3.6 μm or 4.8 μm visibility data. Without introducing scenarios such as inhomogeneities in the dust shell or enhanced forward scattering by grains, the near-infrared visibility curves are best fitted by a dust shell with a larger inner radius since the hottest dust contributes most to the resolved component of the near-infrared visibility curves.

2. The Dyck & Benson and Fix & Cobb 11 μm visibility data both show NML Cyg's dust shell to be much "smaller" than expected for a $\rho \propto r^{-2}$ density distribution with sufficient optical depth to move the silicate feature into absorption. The long-baseline 11.15 μm data alone could be adequately fitted by a uniform outflow model, but such a model can not fit the 11 μm speckle data simultaneously.

In response to the major shortcomings of the uniform outflow models, a series of single shell models were produced in which the dust density behaved as $\rho \propto r^{-5}$. Both the inner radius and optical depth were varied in an attempt to fit the broadest possible set of observations. The choice of dust shell geometry, $\rho \propto r^{-5}$, was based on the results of the previous modeling, where it was observed that the near-infrared emission arose almost entirely in a thin region around the inner radius of the dust shell, because only the hottest of the dust contributes significantly to the visibility curve. This implied that a density distribution falling more steeply than r^{-2} would have little effect on the near-infrared spectrum or visibility curves, but would have the desired effect of shrinking the mid-infrared size, which was dominated by the emission from cool dust (T $\lesssim$ 600 K) far from the star.

Predictions from the $\rho \propto r^{-5}$ dust shell model which fit the most diverse set of observations can be found as the dashed line in Figure 3, while a summary of the model parameters has been placed in Table 4. The best fitted model consisted of a single shell with an inner radius of 110 mas and an 11.15 μm optical depth of 1.93. This model fits most of the observations, including the near-infrared visibility data, mid-infrared speckle observations, the broadband spectrum (above 1 μm), and the mid-infrared silicate feature. Similar quality results were also achieved for steeper density laws, e.g. $\rho \propto r^{-7}$. Hence by allowing the dust shell geometry to deviate from uniform outflow, it was possible to reproduce a much broader range of observations. In fact, this single shell model can explain essentially all the observations, with the sole exception of the long-baseline 11.15 μm visibility data introduced earlier in this paper.

5. Maximum Entropy Reconstruction of the Mid-Infrared Brightness Distribution

The Maximum Entropy Method (MEM), based on the algorithm of Wilczek & Drapatz (1985), was used to reconstruct a circularly symmetric brightness distribution. The 11.4 μm speckle data of Dyck & Benson (1992) were chosen to represent the low resolution data, while the high resolution information was provided by the ISI. Figure 4 contains the MEM reconstruction of the radial profile of NML Cyg, where the brightness distributions plotted are weighted by the radius, so that the area under each curve is proportional to the total monochromatic flux. The MEM fit to the 11 μm visibility points is statistically adequate (χ^2 ~number of degrees of freedom), and is plotted in the inset plot of Figure 4.

Despite the MEM algorithm's attempt to spread the flux out as much as possible in image space while adequately fitting the visibility data, Figure 4 shows evidence for a double shell structure. For comparison, the best-fit uniform outflow model from the previous section (solid line, Figure 3) is included on the figure as the dotted line. The MEM result suggests a two component dust shell geometry with the closest shell appearing approximately 100 mas from the star, similar to the location of the shell in the $\rho_{\rm dust} \propto r^{-5}$ model discussed previously (dashed line, Figure 3).

6. Double Shell Models

With the MEM results it was possible to construct a realistic, two component model which fitted nearly all the observations. Schematically, the two shells consist of one geometrically thin shell located approximately 100 mas from the star (similar to the $\rho \propto r^{-5}$ shell discussed previously), and a distant, colder shell approximately 300 mas from the star. The first shell alone has already been shown to reproduce most of the observations, with the exception of the 11.15 μm observations. The addition of some dust far from the star should have a minimal effect on the near-infrared

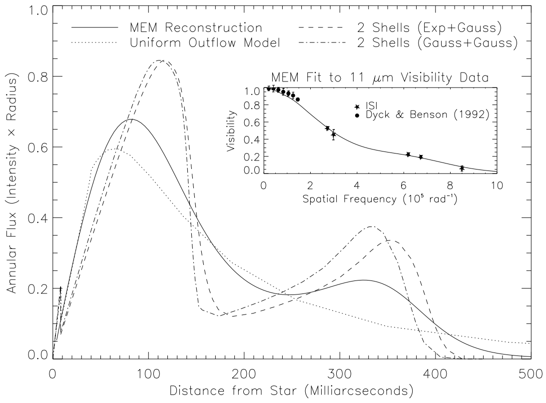

Fig. 4.— The 11 μm annular flux from the Maximum Entropy Method (MEM) reconstruction of NML Cyg is displayed as a solid line, while the visibility data are shown in the inset plot. Only the visibility data taken before 1996 were utilized in the MEM reconstruction. The suggestion of a two-shell geometry is apparent when the MEM result is compared with the results from a uniform outflow model (dotted line). In addition, the calculated annular flux of various dust shell models are included for comparison with the MEM results. The dashed line is from a double shell model where the inner shell dust density is mathematically expressed as an exponential, while the dash-dotted line represents a double shell model in which the inner shell density is described by a radial Gaussian. In both double shell models, the outer shell is described by a radial Gaussian (see Table 4 for model parameters). Note that the annular flux (brightness distribution weighted by the radius) is displayed to make more prominent low surface brightness features which provide significant total flux.

observations because the low temperature dust contributes little to the near-infrared output. However, the MEM reconstruction indicates that such a dust shell can be used to reproduce the high-resolution 11.15 μm visibility data.

The parameterization of the inner dust shell was inspired by David & Papoular (1992). They determined that the dust density distribution around many optically thick IRAS sources could not be modeled with a simple r^{-2} density law, but rather required a geometrically thin, exponential shell near to the star and a uniform density ring far from the star in order to reproduce the observed IRAS colors and deep silicate absorption feature. NML Cyg does not have such a deep silicate feature, but neither is it optically thin at 10 μm.

For convenience, the David & Papoular type distribution was used, with the inner dust shell being described by $\rho \propto exp(-\frac{r-R_{\rm inner}}{l_{\rm scale}})$ for $r > R_{\rm inner}$, where $l_{\rm scale}$ is the 1/e scale height. The density in the outer dust shell had a simple Gaussian radial dependence. The functional form of the dust shell density distribution can be found in Table 4. The scale height of the double shell model used in this analysis was smaller than those used by David & Papoular (1992) because of their numerical code limitations. However, radiative transfer calculations of dust distributions using two Gaussian shells were also performed in order to test the sensitivity of the shell parameters to the chosen density distribution. These results are summarized in Table 4 and will be discussed in the next section. Note that the outer shell found in this paper differs significantly in character from that postulated by David & Papoular (1992). The uniform density shell used in that work was located much farther away from the star than the shell used here, and was primarily useful for fitting the far-infrared flux and the deep absorption found in the silicate feature, two observations not particularly relevant to this study.

Using the MEM reconstruction as a guide, it was straightforward to determine a set of two-shell parameters which fit the 11 μm visibility curve (see Table 4), although such parameters were not unique. In fitting the bump in the 11 μm visibility curve, the possible values of the shell radii and relative optical depths were constrained. The silicate feature was then fitted by adjusting the overall optical depth while keeping the ratio of optical depths roughly the same. As can be seen in Figure 5b, this model provides an excellent fit to the silicate feature. The shape of the silicate fea-

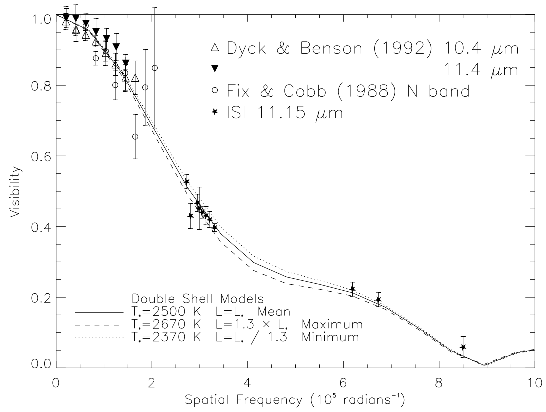

Fig. 5a.— The predictions from a double shell model are presented along with both recent and previously published observations. These results represent NML Cyg at mean luminosity (solid line), maximum luminosity (dashed line), and minimum luminosity (dotted line). (a) Model calculations are compared to observed 11 μm visibility data. Changes in luminosity do not appear to have significant effects on the 11 μm visibility.

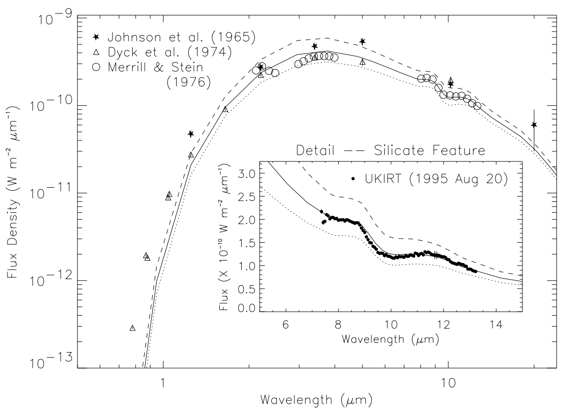

Fig. 5b.— The predictions from a double shell model are presented along with both recent and previously published observations. These results represent NML Cyg at mean luminosity (solid line), maximum luminosity (dashed line), and minimum luminosity (dotted line). (b) The model spectra are compared to broadband and mid-infrared spectral measurements. Note the broadband spectrum is not well-fitted below 1.5 μm. Ossenkopf et al. (1992) dust constants help provide the excellent fit to the silicate feature.

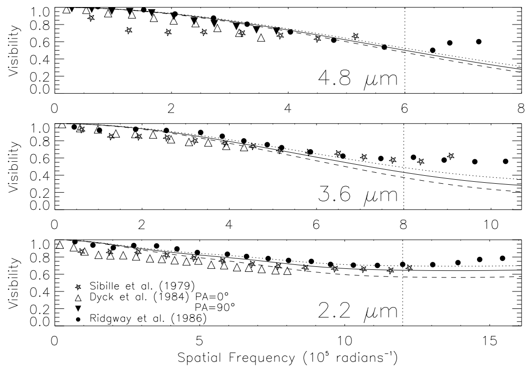

Fig. 5c.— The predictions from a double shell model are presented along with both recent and previously published observations. These results represent NML Cyg at mean luminosity (solid line), maximum luminosity (dashed line), and minimum luminosity (dotted line). (c) Previously published near-infrared visibility measurements near 4.8 μm, 3.6 μm, and 2.2 μm are compared to model calculations. The vertical dotted line represents the spatial frequency cutoff discussed in §3.2. Although fitting the observations well below this cutoff, the models predict high resolution visibility points systematically lower than published observations. These high-resolution values were not fitted in the original publication, and are presumed to be somewhat unreliable.

ture was found to be relatively insensitive to the total optical depth in this region of parameter space, and the 11.15 μm optical depth of the inner shell could be adjusted from 1.8 to 2.5 and still maintain adequate fits to the mid-infrared spectrum and 11 μm visibility data.

Advantage was taken of this parameter flexibility in fitting the broadband spectrum. By decreasing the inner shell's optical depth to 1.8, the previous fits to the silicate feature and 11.15 μm visibility data were maintained while additionally fitting the broadband spectrum for wavelengths longer than $\sim$1.5 μm (see Figure 5b). Possible explanations for this model's failure to fit the spectrum for wavelengths shorter than 1.5 μm are discussed below. Note that this broadband spectrum fit is superior to that achieved by the uniform outflow model in Figure 3b.

Finally, the trial model was compared to the visibility data in the near-infrared. There was little room left for tuning the parameters, because the fits to the broadband spectrum and the mid-infrared data strictly constrained the possible values for the shell inner radii and thicknesses. Furthermore, the overall optical depth of the shells was constrained by the requirement to fit the near-infrared part of the broadband spectrum. The remaining parameter space was exploited in order to optimize the fit to the near-infrared visibility data and the fits for the best double shell model are shown Figure 5c. Clearly the data are fitted adequately by this model, which does not require any arbitrary tuning of optical depths or contributions from an unresolved point source. Residual misfits to the data are as likely to arise from uncertainties in the dust constants, variations in luminosity, or systematic errors in the measurements themselves, as they are from an incorrect model of the dust shell geometry. Probably all of these factors contribute to the residual misfits.

The best fitted double shell model was characterized by an inner shell which began at 120 mas with a scale height of 10 mas. The outer, Gaussian shell was centered around 370 mas with a standard deviation of 20 mas, although this model was not very sensitive to parameters of the outer shell. The respective optical depths of the inner and outer shell at 11.15 μm were 1.8 and 0.34. Given that the density distribution has the correct functional form, the parameters of the inner shell have an approximate uncertainty of 10%, while the outer shell's uncertainties are larger ($\sim$ 20%) because it was not possible to discriminate between a thin shell at 380 mas and a thicker one at 350 mas.

7. Discussion

The two-shell model was tested to see what changes in the simulated spectrum and visibility curves arose due to varying the luminosity and temperature of the star. The temperature of NML Cyg was modeled as 2500 K by Rowan-Robinson & Harris (1983), while Ridgway et al. (1986) used a stellar temperature of 3250 K, appropriate for an M6III star. For a fixed stellar luminosity, changing the effective temperature mainly affects the near-infrared visibility curves. In order to examine the model's sensitivity to the stellar $T_{\rm eff}$, simulations were performed with $T_{\rm eff} = 2500\,{\rm K}$ and 3000 K, while holding the luminosity constant. We found that there was virtually no effect on the fit to the 11 μm visibility data and the broadband spectrum, and that the most significant departure was that the amount of unresolved stellar flux at 2.2 μm increased by $\sim$5% for the lower stellar temperature. As the near-infrared data are not internally consistent to this level, this effect is not considered further.

Since the data collected on NML Cyg were not all from the same epoch, the double shell model discussed above was computed with different stellar luminosities in order to take into account the known variability of this star. Plotted in Figure 5 are model curves for various luminosities of the source, consistent with the maximum and minimum 10 μm flux density from MSSS data (see Figure 1). The change in luminosity was accomplished by fixing the stellar radius and changing only the temperature, which would have exaggerated any temperature effects on the model visibility curves and spectrum. The solid line in Figure 5 represents roughly the mean flux and was used to fit the mid-infrared spectrum taken at UKIRT on 1995 August 20, while the other curves represent models at the maximum and minimum luminosities. Fortunately, the change in luminosity had only a small effect on the mid-infrared visibility predictions, although the 2.2 μm visibility curves were more sensitive. This sensitivity to the stellar luminosity might explain some of the discrepancies in the near-infrared speckle data. Further inconsistencies between NML Cyg observations taken at different times could occur if the dust condensation radius changed significantly during a luminosity cycle. There is currently not enough information to properly model this, however this effect has been seen on other stars such as o Cet (Lopez et al. 1997) and IRC+10216 (Danchi et al. 1994a).

Another check was made to determine the sensitivity of the two-shell model to the detailed geometry of the dust shell. A model similar to the previously discussed two-shell model was created which used an inner Gaussian shell instead of an inner exponential shell. This resulted in only slightly different values for the inner radii and the optical depths, and the best-fit parameters of both double shell models are located in Table 4. Figure 4 compares the 11 μm brightness distribution of both two-shell models with the MEM and uniform outflow results. The 11 μm visibility data predictions from both double shell models can be seen to be nearly identical.

Although successful at explaining a large body of observations, neither single nor double shell models were able to fit the broadband spectrum adequately below 1.5 μm. This is probably due to some combination of the following effects. (1) Interstellar reddening corrections for NML Cyg, which are only very important below 2 μm, are not well known. (2) The relative strengths of the near-infrared dust opacity to the mid-infrared opacity may not be correct (see discussion by OHM [1992] detailing the determination of the near-infrared optical constants). (3) The spectrum could have changed in the last 20 years (see discussion below). (4) Because of the large extinction due to dust in the visible and near-infrared, inhomogeneities in the dust shell could allow additional stellar flux to skew the spectrum. This latter scenario requires $\sim$10% of the 2.2 μm flux to be stellar light unreddened by the dust for the spectrum below 1.5 μm to be adequately fit. Determining which of these scenarios apply will require long-baseline, near-infrared visibility measurements to determine the fraction of light which is stellar.

It is important to emphasize that these models all assume spherical symmetry. However, if non-symmetric models are considered, then the outer shell of the double shell models could be interpreted as a blob or clump of emission with a characteristic distance of 370 mas from the stellar surface. The position angles of the ISI measurements given in Table 1 could be used to investigate possible asymmetric dust distributions, although present data does not encompass sufficient sampling of the Fourier plane to justify full two-dimensional modeling. However, it is interesting to note that the inner and outer shells have similar masses, to within a factor of 2. This suggests that NML Cyg may experience episodic mass ejections, as seen in other supergiants, e.g. α Ori and α Sco. It is expected that the outer shell is beyond the acceleration zone and has attained terminal velocity. The known CO outflow velocity of $\sim$25 km/s allows us to estimate the time between the hypothetical ejections as $\sim$80 years.

To test the hypothesis of episodic mass ejection, a third shell of the same mass was placed around NML Cyg at various radii to see the effect on the 11 μm visibility curves. These radiative transfer results indicated that the small angular size seen by 11 μm speckle observers rule out another such shell within $\sim 1''$. This result is consistent with the Herbig & Lorre (1974) image at 0.8 μm which revealed no nebulosity further than 375 mas from NML Cyg.

The dynamics of the inner shell are not easy to discern. One might expect the inner shell to have condensed out of the gas phase approximately 40 mas from the star, where the temperature was $\sim$1200 K. The assumption that the dust shell was subsequently accelerated to the same velocity as the outflowing CO gas ($\sim$25 km/s) would predict that the inner shell was $\sim$60 mas from the star in 1974, when Merrill & Stein (1976) measured the 2-13 μm spectrum of NML Cyg. Their measurements were averaged over a significant part of the cycle, and hence only a relative spectrum was given. To permit comparison with the present simulations, the spectrum was scaled by a constant factor in order to match the UKIRT observations of 1995 August 20. The scaled results of Merrill & Stein (1976) have been placed on Figures 2, 3b, and 5b, and are consistent with more recent observations. Note the spectral feature seen in the Merrill & Stein spectrum near 2 μm was not included in the numerical computations and does not appear in the model curves. A dust shell model with the inner shell placed approximately 60 mas from the star (but retaining the same functional form and total dust mass) was generated to compare with the silicate feature observed by Merrill & Stein in the early 1970s. The radiative transfer calculation of such a model showed drastic changes in the spectrum and silicate feature inconsistent with spectra given in Figure 2. This indicates that the inner shell has had a velocity substantially lower than 25 km/s, which is consistent with H_2O maser observations discussed below.

The constancy of the silicate feature over the last 20 years suggests other mass-loss scenarios. David & Papoular (1992) envision the optically thick shell as being too heavy to be accelerated away by radiation pressure. Such a shell would presumably continue to collect mass at approximately the same distance from the star until some unusual activity of the star causes a mass ejection. Alternatively, the dust may have formed closer to the star, but is still accelerating and has a smaller velocity than the terminal flow. Considering the uncertainties in the model, the mid-infrared spectra taken 20 years apart are too similar to unambiguously prefer one of these scenarios over another.

Richards et al. (1996) recently presented new measurements of the 22 GHz H_2O maser emission around NML Cyg. These authors found an irregular ring of masers approximately 200 mas across and a pair of features further away, $\sim$600 mas from each other, on either side of the star. The double shell models used in this paper were generated before the Richards et al. (1996) observations were released, and it is interesting to note the similarity in the location of the masers and the twin dust shells derived independently. In addition, proper motions of the distant masers themselves indicate that the masers have velocities consistent with the observed CO gas (19$\pm$4 km/s assuming a distance of 2000 pc). The Doppler velocities of the inner shell of masers indicate that the circumstellar material is gravitationally bound when it enters the H_2O maser region (v$\sim$15 km/s at 50 mas), but leaves the maser zone with a velocity larger than escape velocity (v$\sim$25 km/s at 240 mas). Richards et al. (1996) conclude the inner shell of H_2O masers is still in the acceleration regime.

8. Conclusions

In summary, uniform outflow models of the dust envelope of NML Cyg could not be simultaneously reconciled with both near- and mid-infrared observations. A single, geometrically thin shell of intermediate optical depth can reproduce most of the observations except for the long-baseline, mid-infrared interferometric data. An additional shell of dust was required to fit these high-resolution observations, which are solely sensitive to the relatively low-temperature dust existing hundreds of milli-arcseconds from the stellar surface. Dust shell morphology is important in understanding the possible mechanisms which drive the high mass loss rates observed around red giants. The Ossenkopf, Henning, & Mathis (1992) optical constants were found to be superior to those of David

& Papoular (1990) and of Draine & Lee (1984) in providing model fits to both the detailed shape of the 9.7 μm silicate feature and most of the broadband spectrum. The excess flux observed below 1.5 μm has several possible explanations, although the exact cause is not known.

The double shell models which best fit the observations consist of an inner shell approximately 125 mas from the star with an 11 μm optical depth of $\sim$1.9 and characteristic thickness of $\sim$15 mas. The outer shell was found to reside three times further away with an 11 μm optical depth of $\sim$0.33, and contains roughly the same mass as the inner shell. Although the models were relatively insensitive to the particular dust shell geometry, the exact values of these parameters could change by $\sim$10% depending on the functional form of the dust shell density distributions (see Table 4).

Deviations from spherical symmetry will necessarily change the meaning of the above fits. A dense clump of material 350 mas from the star would be interpreted here as a shell and would cause the inner shell to be modeled thinner than in fact it is. These effects can be important, and confidence in the interpretation should wait until full Fourier (u,v) coverage is obtained.

Coordination of high-resolution observations in the near- and mid-infrared would place the strongest constraints on models of the dust shell geometry and optical constants. A factor of 2 improvement in resolution will allow for the near-infrared observations to fully resolve the dust and thus yield a measurement of the fraction of stellar flux escaping the envelopes directly. These data should be available in the future as a new generation of multi-element infrared interferometers become operational. Dynamical simulations of red giant atmospheres will be required to fully interpret such new observational data. The U.C. Berkeley Infrared Spatial Interferometer will continue to observe NML Cyg on a regular basis.

We thank W.-H. Tham and C.D. Matzner for enlightening discussions. N. Turner and J. Graham were both helpful in obtaining the most recent reddening curves, and V. Ossenkopf and P. David graciously provided computer-readable versions of their optical constants. Long-baseline interferometry in the mid-infrared at U.C. Berkeley is supported by the National Science Foundation (Grants AST-9321384, AST-9321289, & AST-9500525) and by the Office of Naval Research (OCNR N00014-89-J-1583 & FDN0014-96-1-0737). M. J. was supported under the auspices of the U.S. Department of Energy by Lawrence Livermore National Laboratory under Contract W-7405-ENG-48. E. L. was supported by a National Science Foundation graduate fellowship during part of this work. The United Kingdom Infrared Telescope is operated by the Joint Astronomy Centre on behalf of the U.K. Particle Physics and Research Council.

REFERENCES

Bester, M., Danchi, W. C., & Townes, C. H. 1990, in Amplitude and Intensity Spatial Interferometry, ed. J. B. Breckinridge, Proc. SPIE 1237, 40

Bester, M., Danchi, W. C., Degiacomi, C. G., & Bratt, P.R. 1994, in Amplitude and Intensity Inteferometry II, ed. J. B. Breckinridge, Proc. SPIE 2200, 274

Bowers, P. F., Johnston, K. J., & Spencer, J. H. 1983, ApJ, 274, 733

Danchi, W. C., Bester, M., Degiacomi, C.G., & Townes, C. H. 1990, ApJ, 359, L59

Danchi, W. C., Bester, M., Degiacomi, C. G., Greenhill, L. J., & Townes, C. H. 1994a, AJ, 107, 1469

Danchi, W. C., Bester, M., Greenhill, L. J., Degiacomi, C. G., & Townes, C. H. 1994b, in Amplitude and Intensity Spatial Interferometry II, ed. J. B. Breckinridge, Proc. SPIE 2200, 286

David, P., & Papoular, R. 1990, A&A, 237, 425

———. 1992, A&A, 265, 195

Draine, B. T., & Lee, H. M. 1984, ApJ, 285, 89

Dyck, H. M., Lockwood, G. W., & Capps, R. W. 1974, ApJ, 189, 89

Dyck, H. M., Zuckerman, B., Leinert, C., & Beckwith, S. 1984, ApJ, 287, 801

Dyck, H. M., & Benson, J. A. 1992, ApJ, 104, 377

Fix, J. D., & Cobb, M. L. 1988, ApJ, 329, 290

Fleischer, A. J., Gauger, A., & Sedlmayr, E. 1995, A&A, 297, 543

Herbig, G. H., & Lorre, J. 1974, ApJ, 189, 73

Johnson, H. L., Low, F. J., & Steinmetz, D. 1965, ApJ, 142, 808

Knapp, G. R., Phillips, T. G., Leighton, R. B., Lo, K. Y., Wannier, P.G., & Wooten, H. A. 1982, ApJ, 252, 616

Lee, T. 1970, ApJ, 162, 217

Lopez, B., Danchi, W. C., Bester, M., Hale, D. D. D. S., Lipman, E. A., Monnier, J. D., Tuthill, P. G., Townes, C. H., Degiacomi, C. G., Geballe, T. R., Greenhill, L. J., Cruzalebes, P., Lefevre, J., Mekarnia, D., Mattei, J. A., Nishimoto, D., & Kervin, P. W. 1997, ApJ, in press

Mathis, J. S., Rumpl, W., & Nordsieck, K. H. 1977, ApJ, 217, 425

Mathis, J. S. 1990, ARA&A, 28, 37

Merrill, K. M., & Stein, W. A. 1976, PASP, 88, 294

Morris, M., & Jura, M. 1983, ApJ, 267, 179

Nishimoto, D., Kissel, K. E., Africano, J. L., Lambert, J. V., & Kervin, P. W. 1995, "The Maui Space Surveillance Site Infrared Calibration Sources," Technical Report, unpublished

Ossenkopf, V., Henning, T., & Mathis, J. S. 1992, A&A, 261, 567

Ridgway, S. T., Joyce, R. R., Conners, D., Pipher, J. L., & Dainty, C. 1986, ApJ, 302, 662

Richards, A. M. S., Yates, J. A., & Cohen, R. J. 1996, MNRAS, 282, 665

Rowan-Robinson, M. 1982, MNRAS, 201, 281

Rowan-Robinson, M., & Harris, S. 1983, MNRAS, 202, 767

Sibille, F., Chelli, A., & Lena, P. 1979, A&A, 79, 315

Strecker, D. W. 1975, AJ, 80, 451

Toon, O. B., & Ackerman, T. P. 1981, Appl. Opt., 20, 3657

Wilczek, R., & Drapatz, S. 1985, A&A, 142, 9

Winters, J. M., Fleischer, A. J., Gauger, A., & Seldmayr, E. 1994, A&A, 290, 623

———. 1995, A&A, 302, 483

Wolfire, M. G., & Cassinelli, J. P. 1986, ApJ, 310, 207

TABLE 1
ISI JOURNAL OF OBSERVATIONS

Date	Spatial Frequency (10^5 rad^{-1})	Visibility	Position Angle[a] (Degrees)
1994 Sep 22	2.73	0.53 ± 0.02	50 ± 10
1996 Oct 10	2.81	0.43 ± 0.03	50 ± 3
1996 Sep 23, Oct 10	2.95	0.47 ± 0.03	56 ± 2
1994 Sep 15	2.99	0.45 ± 0.06	58 ± 2
1996 Sep 23, Oct 10	3.05	0.44 ± 0.02	60 ± 2
1996 Sep 23, Oct 7,10	3.13	0.43 ± 0.03	63 ± 1
1996 Oct 7,10	3.21	0.42 ± 0.02	66 ± 2
1996 Oct 7,10	3.31	0.40 ± 0.01	70 ± 2
1993 Sep 30	6.19	0.22 ± 0.02	93 ± 3
1993 Sep 30	6.73	0.19 ± 0.02	97 ± 3
1993 Jul 27	8.50	0.059 ± 0.030	140 ± 5
1994 Jul 8,9,14	27.5	< 0.07	130 ± 20

[a]Position angle is measured in degrees East of North

TABLE 2
JOURNAL OF UKIRT PHOTOMETRY AT 11.15 μM

Date	Flux (10^{-12} Wm$^{-2}\mu$m^{-1})	Flux (10^3 Jy)
1991 Sep 12	141 ± 14	5.9 ± 0.6
1992 Aug 19	122 ± 12	5.1 ± 0.5
1994 Aug 26	114 ± 6	4.74 ± 0.24
1994 Nov 20	97 ± 19	4.0 ± 0.8
1995 Mar 17	104 ± 5	4.30 ± 0.22
1995 Aug 08	125 ± 13	5.2 ± 0.5
1995 Dec 02	122 ± 12	5.0 ± 0.5

TABLE 3
JOURNAL OF SPECKLE OBSERVATIONS

Date	λ (μm)	$\Delta\lambda$ (μm)	Position Angle (Degrees)	Reference
1978	2.2	0.09	120	Sibille et al. 1979
May 20	3.5	0.57	120	
	4.7	0.21	120	
1981-1983	2.2	0.4	0	Dyck et al. 1984
	3.8	0.6	0	
	4.8	0.5	0,90	
1983	2.2	0.1	0,90	Ridgway et al. 1986
Jun 29-30	3.45	0.57	0,45,90	
	4.95	0.5	0	
1985	10	5.0	0	Fix & Cobb 1988
Jul 21-22				
1988-1989	10.4	1.0	0	Dyck & Benson 1992
	11.4	1.0	0	

TABLE 4
MODEL PARAMETERS

Model Description	R_* (mas)	T_* (K)	Shell One Parameters	Shell Two Parameters	Comments
Single Shell: Uniform Outflow	8.6	2500	$\rho \propto r^{-2}$ $R_{\rm inner} = 40$ mas $\tau_{11} = 2.4$		Fits 11 μm visibility. Poor fit to 4.8 μm speckle data and broadband spectrum.
Single Shell: Geometrically Thin	8.6	2500	$\rho \propto r^{-5}$ $R_{\rm inner} = 110$ mas $\tau_{11} = 1.93$		Fits all data except for long-baseline 11 μm interferometry
Double Shell: Exponential & Gaussian	8.2	2500	$\rho \propto e^{-(r-R_1)/l}$ R_1 =120 mas $l = 10$ mas $\tau_{11} = 1.8$	$\rho \propto e^{-\left[\frac{(r-R_2)}{\sigma_2}\right]^2}$ R_2 =370 mas $\sigma_2 = 20$ mas $\tau_{11} = 0.34$	Fits all data except spectrum below 2 μm
Double Shell: Gaussian & Gaussian	8.2	2500	$\rho \propto e^{-\left[\frac{(r-R_1)}{\sigma_1}\right]^2}$ R_1 =125 mas $\sigma_1 = 10$ mas $\tau_{11} = 2.0$	$\rho \propto e^{-\left[\frac{(r-R_2)}{\sigma_2}\right]^2}$ R_2 =350 mas $\sigma_2 = 20$ mas $\tau_{11} = 0.33$	Fits all data except spectrum below 2 μm